

Cite this: DOI: 10.1039/c1nr11033k

www.rsc.org/nanoscale

PAPER

Enhanced photocatalytic activity of hierarchical ZnO nanoplate-nanowire architecture as environmentally safe and facilely recyclable photocatalyst

Feng Xu,^a Yuting Shen,^a Litao Sun,^{*a} Haibo Zeng^b and Yinong Lu^c

Received 5th August 2011, Accepted 14th September 2011

DOI: 10.1039/c1nr11033k

A hierarchical ZnO nanoplate-nanowire (ZNP-ZNW) architecture immobilized onto a substrate *via* a facile two-step synthesis strategy was used as an environmentally safe and recyclable photocatalyst. It showed greatly enhanced photocatalytic activity compared with a monomorphological ZnO nanoplate structure in the degradation of methyl orange (MO). The higher content of surface oxygen defects, which can capture the photogenerated electrons and holes separately and make them available for decomposing organic contaminants, is considered to play an important role in the degradation of MO and makes a major contribution to the enhanced photocatalysis. Increasing the surface-to-volume (S/V) ratio without limit cannot benefit the photocatalytic activity significantly if there are not enough defects to separate additional photogenerated charges caused by a larger S/V ratio. A detailed photocatalytic mechanism related to surface defects of the hierarchical architecture was clearly demonstrated. The present study provides a new paradigm for further understanding the photocatalytic mechanism and suggests a new direction to design high-efficiency photocatalysts based on increasing the number of surface defects of nanostructures.

1. Introduction

At present, environmental pollution has become a major threat to the lives of humans. Pollutants, especially from polluted air and industry effluents, pose a severe ecological problem as the bio-degradation of these pollutants is generally very slow and conventional treatments are mostly ineffective and not environmentally benign. Photocatalytic purification by semiconducting oxides of organic pollutants from industrial wastewater shows great promise for environmental remediation due to their peculiar and fascinating physicochemical properties,^{1–4} allowing the “green” mineralization of organic pollutants. ZnO is just a case in point. By considering that under light irradiation, photocatalytic reactions mainly take place on the surface of the catalyst, a nanoscale ZnO material is believed to perform much better than its bulk counterpart in photolysis processes thanks to a higher surface-to-volume (S/V) ratio. Moreover, when the size of the catalyst reaches the nanoscale, the probability of recombination of photo-generated electron-hole pairs diminishes owing to their fast arrival at reaction sites on the surface.⁵ Therefore, much effort has been devoted to the controlled

synthesis of various nanoscale ZnO structures with high S/V ratio.^{6–12}

In terms of practical photocatalytic applications, nanostructures that are stable against excessive aggregation and possess a higher S/V ratio are paramount for highly efficient photocatalytic degradation of organic pollutants in wastewater. However, ZnO nanostructured photocatalysts are generally used in a suspended state in water,¹³ which could result in excessive aggregation and thus in a dramatic decrease of the active surface area. In addition, this utilization has another drawback of requiring separation and recovery of the photocatalyst from the liquid after completion of the degradation process, which inevitably increases the operating cost. Otherwise, the uncontrolled release of nanoscale photocatalysts to the natural environment not only leads to wasting of the photocatalysts but also induces environmental safety concerns to some extent. For instance, some engineered nanomaterials (TiO₂, ZnO, Ag, CNT, fullerenes) represent a potential health hazard to living organisms.^{14–16}

The alternative to a suspension is to use the photocatalyst in an immobilized form (films). For instance, ZnO nanotape arrays synthesized on a Si wafer by a thermal evaporation process, rather than unsupported nanoscale powders, have been used as a photocatalyst.¹⁷ Although this method can indeed solve the separation problem and offers some degree of recyclability, owing to their high cost and unavailability on a large scale, these materials are unsuitable for industrial mass production. Very recently, Wang *et al.*¹⁸ reported that ZnO nanorod (ZNR) arrays fabricated directly on Zn foil *via* a simple self-sourced growth approach also show good recyclability. Into the bargain,

^aSEU-FEI Nano-Pico Center, Key Laboratory of MEMS of Ministry of Education, Southeast University, Nanjing, 210096, China. E-mail: slt@seu.edu.cn; Fax: +86-25-83790873; Tel: +86-25-83790573

^bInternational Center for Materials Nanoarchitectonics (MANA), National Institute for Materials Science (NIMS), Namiki 1-1, Tsukuba, Ibaraki, 305-0044, Japan

^cState Key Laboratory of Materials-Oriented Chemical Engineering, Nanjing University of Technology, Nanjing, 210009, China

large-scale fabrication of quasi-aligned stacking nanoplates (ZNPs) immobilized on substrates have also been realized and used in photocatalysis.¹⁹ Nevertheless, further increasing the S/V ratio of ZNP films is still of great necessity.

In this regard, we report for the first time on the photocatalytic performance of a hierarchical ZnO nanoplate-nanowire (ZNP-ZNW) architecture with a high S/V ratio achieved *via* a facile two-step synthesis route. The two-step approach is based on firstly a low-temperature aqueous electrodeposition of the ZNP array, and secondly an aqueous chemical growth (ACG) of branched ZNWs on the surface of the ZNPs. The hierarchical nanostructure in the form of an immobilized film on a removable substrate can be conveniently reused and shows a remarkable improvement of the photocatalytic activity in the photodegradation of MO compared with pure ZnO nanoplates. In addition, the effects of surface nanofeatures and defects of the as-synthesized ZnO samples on the photocatalytic activity were investigated to explore the reason for the enhanced photocatalytic performance of the ZnO samples, and further understand the photocatalytic mechanism.

2. Experimental section

The hierarchical ZNP-ZNW architecture with high S/V ratio were produced on a large scale *via* a facile two-step synthesis approach. Typically, in the first step, large-scale ZNP arrays were electrodeposited on indium tin oxide (ITO, In:SnO₂) glass substrates (10 Ω \square^{-1}) in an aqueous electrolyte of 0.05 M Zn(NO₃)₂ and 0.1 M KCl with a three-electrode electrochemical configuration that can be found elsewhere.^{20,21} In brief, an ITO substrate, a Pt electrode, and a saturated calomel electrode (SCE) were used as the working electrode, the counter electrode, and reference electrode, respectively. The electrodeposition was performed at -1.1 V and 70 °C for 30 min. In the second step, an aqueous chemical growth (ACG) method²² was adopted to grow branched ZNWs on the surface of the ZNPs by immersing the ZnO nanoplate substrate obtained from the first step into a bottle filled with an equimolar concentration (0.01 M) aqueous solution of Zn(NO₃)₂ and C₆H₁₂N₄. The bottle was sealed and kept at a constant temperature of 90 °C. Finally, the hierarchical ZNP-ZNW architecture immobilized on the ITO substrate was obtained and then used for further characterization by a scanning electron microscope (SEM, JSM-5900), an X-ray diffractometer (XRD, ARL XTRA), and a spectrophotometer (Jobin Yvon Fluorolog3-221) with a Xe lamp (450 W) as excitation source at an excitation wavelength of 325 nm.

The photocatalytic activities of the as-prepared ZNP array and hierarchical ZNP-ZNW architecture were evaluated by decomposing methyl orange (MO) in aqueous solution under UV irradiation of a 300 W high-pressure Hg lamp (the strongest emission at 365 nm) using a self-made photodegradation setup, as shown in Fig. 1. In a typical experiment, the ITO-supported samples were horizontally immersed in the organic dye solution (20 mL, 6.0×10^{-5} M). The exposed zone (4 cm²) for dye photodegradation was in the face of the upper UV lamp (distance = 25 cm), and the intensity of UV irradiation was around 8 mW cm⁻². Before irradiation, the aqueous solution was magnetically stirred in the dark for 20 min to reach the adsorption and desorption equilibrium of organic dyes with the catalyst. UV-Vis

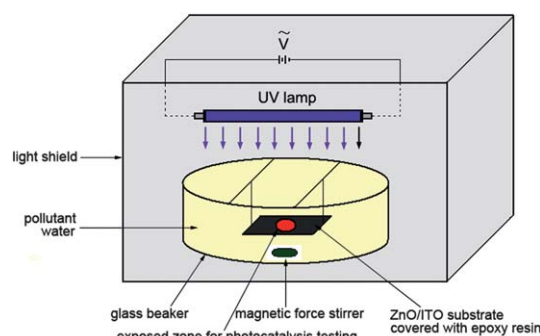


Fig. 1 Schematic diagram of the photodegradation setup of organic pollutants in wastewater.

absorption spectra monitoring the change in concentration of the organic dyes were periodically recorded using a Shimadzu UV-3101PC UV-vis-NIR spectrophotometer. The residual dye content was calculated as A/A_0 , where A and A_0 are the absorbance values corresponding to the tested and the original control solution, respectively.

3. Results and discussion

The hierarchical ZNP-ZNW architecture derived from the ZNP array is characterized by SEM, as shown in Fig. 2. Fig. 2a shows the pristine ZNP array firstly electrodeposited on the ITO substrate on a large scale at a low temperature of 70 °C. These ZNPs standing vertically on the substrate exhibit regular hexagonal end planes and are 2–3 μm in diameter and about 100 nm in thickness. The magnified image (inset in Fig. 2a) further demonstrates that the surface of the pristine ZNPs is quite smooth, and there are gaps existing among the vertically aligned plate-like crystals. Subsequently, the ACG method was used to grow branched ZNWs on the ZNPs. Fig. 2b reveals that the suitably grown ZNP-ZNW architecture was obtained after a 12 h aqueous chemical growth, and densely and randomly oriented ZNWs derived from the ZNPs are outstretched to fill the intervals among the primary ZNPs. This greatly increases the S/V ratio of the original ZNP array film. Closer observation (inset in Fig. 2b) reveals that most of the ZNWs preferentially grew at the brims of the ZNPs. According to recent investigations on the growth mechanism of branched ZNRs on the surface of ZNR,^{23,24} our hierarchical ZNP-ZNW architecture should likewise be ascribed to ZnO secondary nucleation and sequential growth on primary ZNPs. A structural analysis of the

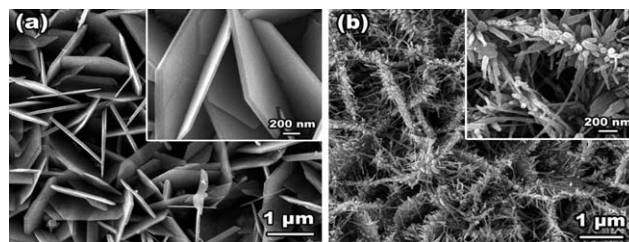


Fig. 2 SEM images of (a) the ZNP array and (b) the hierarchical ZNP-ZNW architecture derived from the ZNP array. The insets show magnified images for clearer differentiation.

hierarchical ZNP-ZNW architecture has been carried out using XRD. Fig. 3, the XRD pattern of the hierarchical ZNP-ZNW architecture, proves its ZnO hexagonal wurtzite structure. No characteristic peaks of other impurities were detected in the pattern, suggesting that only single-phase ZnO was formed by the ACG method.

ZnO is a promising kind of photocatalyst for dye degradation due to its high photosensitivity and wide band gap of 3.37 eV. In previous reports,^{25,26} ZNPs synthesized by methods other than electrodeposition have shown superior photocatalytic activity to nanoscale ZnO particles. Herein, to further demonstrate the potential applicability of the hierarchical ZNP-ZNW architecture for the removal of organic contaminations from wastewater, we investigated their photocatalytic activity *versus* the ZNP arrays by employing the photocatalytic degradation of methyl orange (MO) at ambient temperature. Fig. 4 shows the adsorption spectra of an aqueous solution of MO (initial concentration of 6.0×10^{-5} M, 20 mL), respectively, in the presence of the ITO substrate-supported ZNP arrays and hierarchical ZNP-ZNW architecture under exposure (4 cm²) to UV light irradiation for different periods of time. As shown in Fig. 4a, the characteristic adsorption peak corresponding to MO molecules at 464 nm gradually decreased in intensity with increasing exposure time and ultimately vanished after a long time of 90 min, implying the nearly complete photodegradation of MO under the photocatalytic action of the ZNP arrays. No newly appearing adsorption peaks are visible in the whole spectrum. When the hierarchical ZNP-ZNW architecture was used as a catalyst to photodegrade MO in aqueous solution, similar changes in the adsorption peak were observed too, the difference being the shorter time required (50 min) for complete degradation of MO, as shown in Fig. 4b.

Further comparative results shown in Fig. 5a clearly indicate the obvious contrast in degradation rate of MO for the two ZnO samples. The control experiment in the absence of ZnO photocatalyst but under identical UV irradiation was also illustrated and only a slight concentration decrease for MO in the solution was observed after 120 min. However, in the case of the hierarchical ZNP-ZNW architecture, it only took about 50 min to achieve complete degradation of MO, in great contrast to 90 min for the ZNP arrays, therefore showing a photocatalytic efficiency enhanced by around 80% compared with the monomorphological ZNP arrays. Moreover, compared with the reported powdery ZnO photocatalysts generally used in a suspended state in water, our as-synthesized hierarchical

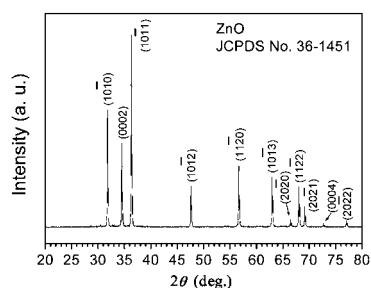


Fig. 3 XRD pattern of the hierarchical ZNP-ZNW architecture derived from the as-electrodeposited ZNP array.

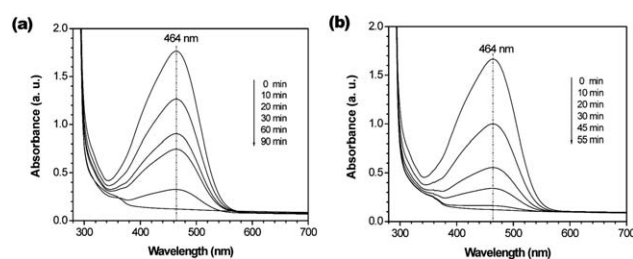


Fig. 4 Adsorption spectra of methyl orange solutions in the presence of (a) the ZNP arrays and (b) the hierarchical ZNP-ZNW architecture under exposure to UV light.

ZNP-ZNW architecture immobilized on an ITO substrate has better structure stability due to facile recyclability. Thus, stable photocatalytic activity can be maintained even after seven cycles (see Fig. 5b).

It is well known that a larger *S/V* ratio benefits the photocatalytic activity as it allows more organic substances to be attached to the surface of the photocatalyst. Here, our hierarchical ZNP-ZNW architecture also has a larger *S/V* ratio in comparison with the ZNP arrays, since the intervals among the adjacent ZNP arrays have been filled with the bushy ZNWs (see Fig. 2b). The calculation of the *S/V* ratio based on the fact that most of ZNWs grew at the brims of ZNPs demonstrates that the hierarchical ZNP-ZNW architecture has a *S/V* ratio over three times higher than the ZNP arrays provided that 100 ZNWs of average 50 nm in diameter and 500 nm in length grow on 1 μm² ZNP surface. Apparently, the photocatalytic efficiency (80%) is not proportional to the increase in *S/V* ratio, as encountered in the case of powdery ZnO photocatalysts²⁷ and other kinds of oxide photocatalysts.²⁸ For instance, even though ZnO nanotubes have a *S/V* ratio over 10 times higher than ZnO particles, the former only shows an enhancement in photocatalytic efficiency of around 100% compared with the latter.²⁷ An increased *S/V* ratio could even result in an unusual decrease in photocatalytic activity.^{28–30} These results indicate that increasing the *S/V* ratio without limit cannot afford an equivalent enhancement in the photocatalytic efficiency. Increasing the *S/V* ratio only provides the probability of yielding more photon-generated electrons and holes, but cannot effectively prevent their recombination that could result in significant degeneration of photocatalytic activity. Therefore, simply pursuing a higher *S/V*

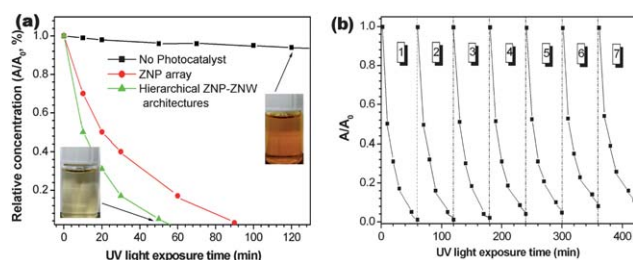


Fig. 5 (a) Photodegradation kinetics of MO solutions in the presence of the ZNP array and the hierarchical ZNP-ZNW architecture under exposure to UV light. The control experiment without ZnO photocatalyst is also displayed. (b) Cyclic photodegradation of MO solutions only in the presence of the hierarchical ZNP-ZNW architecture for seven cycles.

ratio is not the only resort for greatly advancing the photocatalytic efficiency. Other factors that influence the photocatalytic activity should be further exploited to account for the enhanced photocatalytic efficiency of our hierarchical architecture.

Generally, besides the above-mentioned S/V ratio that can markedly influence the photocatalytic performance of the samples, surface defects (especially oxygen defects) of the samples are also considered to be a paramount factor that is directly responsible for enhancing photocatalytic activities.³¹ A study of the room-temperature photoluminescence (PL) spectrum is an effective technique to evaluate surface defects of ZnO samples. In the PL spectra of ZnO, typically there are emission bands in the ultraviolet (UV) and visible (green, yellow, blue, and violet) regions. Fig. 6 shows the room-temperature PL spectra of the ZNP array and hierarchical ZNP-ZNW architecture, respectively. Both the ZnO samples display a similar ultraviolet (UV) emission peak with maximal intensity at around 376 nm, which is due to the excitonic recombination of the photo-generated holes in the valence band and the electrons in the conduction band.^{32–34} However, as for the visible emissions, no similar emission peak positions are observed for the two ZnO samples. Generally speaking, ZnO exhibits luminescence in the visible spectral range owing to intrinsic or extrinsic defects.³⁵ Nevertheless, the exact origins of the visible emissions are currently still highly controversial and ambiguous. For example, many different hypotheses have been proposed to explain the green emission, such as recombination of photogenerated holes with singly ionized oxygen vacancies (V_O),^{36,37} recombination between electrons close to the conduction band and deeply trapped holes at a V_O center,^{38,39} surface defects,⁴⁰ etc. Moreover, the yellow and blue emissions are considered to be related to interstitial oxygen⁴¹ and interstitial zinc,⁴² respectively. Here, our as-electrodeposited ZNP array exhibits a broad and weak blue-green emission centered at about 490 nm, whereas the hierarchical ZNP-ZNW architecture derived from the original ZNP array shows a broad and strong green-yellow emission (575 nm), which indicates evolution of the defect from coexisting interstitial zinc and oxygen vacancies in the pristine ZNP array to coexisting oxygen vacancies and interstitial oxygen in the hierarchical ZNP-ZNW architecture. It is worth noting that the intensity of the blue-green emission peak in ZNP PL is far from that of the green-yellow emission peak in the hierarchical ZNP-ZNW architecture PL, indicating more surface oxygen defects in the latter. Based on the large variation in visible emission peaks observed in the PL

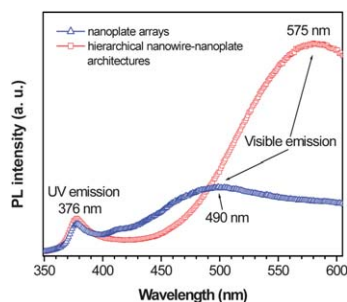
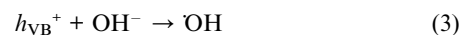
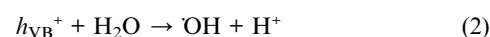
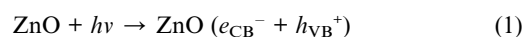


Fig. 6 Room-temperature PL spectra of the ZNP arrays and the hierarchical ZNP-ZNW architecture.

spectra, it is concluded that the two-step synthesis approach resulted in more surface oxygen defects in the hierarchical ZNP-ZNW architecture which could greatly enhance the photocatalytic activity.

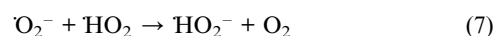
To better analyze the discrepancy in photocatalytic activity resulting from the difference in surface nanofeatures of the ZnO samples, it is of great necessity to understand the photocatalytic mechanism of the semiconductor. It is generally accepted that when ZnO nanocrystals are irradiated by UV light with a photon energy $h\nu$ that matches or exceeds the bandgap energy (E_g) of ZnO, electrons (e_{CB}^-) can be excited from the valence band (VB) to the conduction band (CB), simultaneously leaving the same number of holes (h_{VB}^+) behind in the VB (eqn (1)).⁴³ Matthews⁴⁴ has suggested that reaction of the valence-band holes with either adsorbed H_2O or with the surface OH^- groups on the semiconductor particles is the major route of formation of hydroxyl radicals (OH) (eqn (2) and 3):



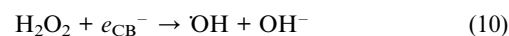
Izumi *et al.*⁴⁵ suggested that these $\cdot OH$ radicals form not only *via* the valence-band holes but also *via* H_2O_2 from $\cdot O_2^-$ groups. It is generally accepted that oxygen plays an important role in semiconductor-mediated reactions by trapping the conduction-band electron as superoxide anions (O_2^-) and thus delaying the electron-hole recombination process:



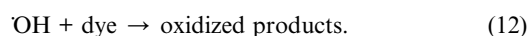
H_2O_2 can be formed from $\cdot O_2^-$ *via* eqn (5)–(8):



Cleavage of H_2O_2 by any of the reactions in eqn (9)–(11) may generate $\cdot OH$ radicals:



These $\cdot OH$ radicals which are extremely strong oxidants can result in the partial or complete mineralization of deleterious organic substances such as dye in the wastewater (eqn (12)):



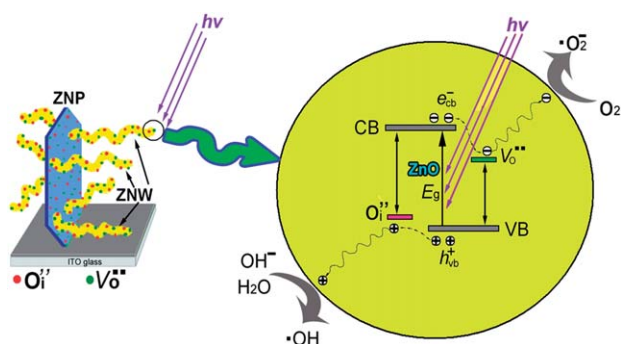


Fig. 7 Schematic diagram showing the surface oxygen defect-related photocatalytic mechanism of the hierarchical ZnO nanoplate-nanowire architecture.

However, the photon-generated electrons and holes could also recombine and dissipate the input energy as heat, leading to a decrease in the photocatalytic efficiency. This commendably interprets the phenomena met by us and other researchers,^{27–30} *i.e.*, increasing the S/V ratio cannot equivalently enhance and may even deteriorate the photocatalytic activity. If a suitable scavenger or surface defect state is available to trap the electrons or holes, undesirable recombination can be prevented effectively. For instance, oxygen vacancies (V_{O}) can trap the photon-generated electrons temporarily to reduce the surface recombination of electrons and holes; whereas interstitial oxygen (O_{i}) could serve as shallow trappers of photon-generated holes to restrain the recombination of electrons and holes.^{46,47} The proposed band structure and photocatalytic mechanism of ZnO nanocrystals with different kinds of surface oxygen defects are schematically illustrated in Fig. 7.^{6,42,43} As the redox reactions might occur on the surface of the V_{O} and O_{i} defects, the oxygen defects can be considered to be the active sites of the ZnO photocatalyst.

According to the above discussions based on PL characterization and SEM observations, it is concluded that compared with the ZNP arrays, the hierarchical ZNP-ZNW architecture has more surface oxygen defects and a larger S/V ratio factor that jointly result in better photocatalytic activity. More significantly, our two-step synthetic approach can produce ZnO nanostructures on a large-scale in the form of immobilized films on removable substrates, which effectively solves the separation issue and avoids the release of nanoscale catalysts into the natural environment. In addition, the recovery of the catalysts can make them recyclable, resulting in a low economic cost. Therefore, this synthetic approach to hierarchical nanostructured ZnO photocatalysts directly immobilized on substrates is compatible with industrial feasibility in practical use and environmental protection due to the decreased release of nanoscale materials to the natural environment.

4. Conclusions

In conclusion, we demonstrate that the hierarchical ZNP-ZNW architecture can be immobilized on a removable substrate *via* a facile two-step synthesis approach. The ZnO nanostructure in the form of an immobilized film can act as a highly efficient

photocatalyst and is recyclable in the present studies involving photodegradation of MO solutions due to avoiding the drawback of requiring separation and recovery of the photocatalysts from liquid wastewater. Further control results indicate that compared with the ZNP arrays, the higher photocatalytic activity of the hierarchical ZNP-ZNW architecture cannot simply be ascribed to a larger S/V ratio. The major contribution is from the larger surface oxygen defects which can capture the photogenerated electrons and holes separately and make them available for decomposing organic contaminants. This work suggests a new direction to improve photocatalysis of nanostructures based on increasing the number of surface defects. Moreover, our synthetic approach also pays attention to both the economic cost and environmental safety concerns that arise from the release of nanoscale materials into the natural environment.

Acknowledgements

This work was supported by the National Basic Research Program of China (973 Program, Grant Nos. 2011CB707601 and 2009CB623702), the National Natural Science Foundation of China (NNSFC, Grant Nos. 61106055, 51071044, 60976003 and 61001044), China Postdoctoral Science Foundation Funded Project (Grant No. 20100470066), Jiangsu Planned Projects for Postdoctoral Research Funds (Grant No. 0902003B), and **Open Research Fund of State Key Laboratory of Bioelectronics**.

References

- G. Liu, H. G. Yang, X. W. Wang, L. N. Cheng, H. F. Lu, L. Z. Wang, G. Q. Lu and H. M. Cheng, *J. Phys. Chem. C*, 2009, **113**, 21784.
- M. Liu, L. Y. Piao, W. M. Lu, S. T. Ju, L. Zhao, C. L. Zhou, H. L. Li and W. J. Wang, *Nanoscale*, 2010, **2**, 1115.
- N. Morales-Flores, U. Pal and E. S. Mora, *Appl. Catal., A*, 2011, **394**, 269.
- X. F. Chen, X. C. Wang and X. Z. Fu, *Energy Environ. Sci.*, 2009, **2**, 872.
- Q. Wan, T. H. Wang and J. C. Zhao, *Appl. Phys. Lett.*, 2005, **87**, 083105.
- Y. G. Chang, J. Xu, Y. Y. Zhang, S. Y. Ma, L. H. Xin, L. N. Zhu and C. T. Xu, *J. Phys. Chem. C*, 2009, **113**, 18761.
- B. Weintraub, Z. Z. Zhou, Y. H. Li and Y. L. Deng, *Nanoscale*, 2010, **2**, 1573.
- H. Q. Wang, G. H. Li, L. C. Jia, G. Z. Wang and C. J. Tang, *J. Phys. Chem. C*, 2008, **112**, 11738.
- C. Li, G. J. Fang, F. H. Su, G. H. Li, X. G. Wu and X. Z. Zhao, *Appl. Phys. Lett.*, 2007, **90**, 033107.
- F. Xu, Y. N. Lu, L. T. Sun and L. J. Zhi, *Chem. Commun.*, 2010, **46**, 3191.
- X. Y. Xue, Z. H. Chen, L. L. Xing, C. H. Ma, Y. J. Chen and T. H. Wang, *J. Phys. Chem. C*, 2010, **114**, 18607.
- W. Chen, H. F. Zhang, I. M. Hsing and S. H. Yang, *Electrochem. Commun.*, 2009, **11**, 1057.
- M. Ziegmann and F. H. Frimmel, *Water Sci. Technol.*, 2010, **61**, 273.
- B. D. Johnston, T. M. Scown, J. Moger, S. A. Cumberland, M. Baalousha, K. Linge, R. V. Aerle, K. Jarvis, J. R. Lead and C. R. Tyler, *Environ. Sci. Technol.*, 2010, **44**, 1144.
- F. Gottschalk, T. Sonderer, R. W. Scholz and B. Nowack, *Environ. Sci. Technol.*, 2009, **43**, 9216.
- N. M. Franklin, N. J. Rogers, S. C. Apte, G. E. Batley, G. E. Gadd and P. S. Casey, *Environ. Sci. Technol.*, 2007, **41**, 8484.
- Z. B. He, Y. Jiang, W. J. Zhang, J. A. Zapien, Y. Liu, W. F. Zhang and I. Bello, *Phys. Status Solidi A*, 2009, **206**, 94.
- Y. X. Wang, X. Y. Li, G. Lu, X. Quan and G. H. Chen, *J. Phys. Chem. C*, 2008, **112**, 7332.

- 19 X. L. Cao, H. B. Zeng, M. Wang, X. J. Xu, M. Fang, S. L. Ji and L. D. Zhang, *J. Phys. Chem. C*, 2008, **112**, 5267.
- 20 F. Xu, Y. N. Lu, Y. Xie and Y. F. Liu, *Mater. Des.*, 2009, **30**, 1704.
- 21 L. F. Xu, Y. Guo, Q. Liao, J. P. Zhang and D. S. Xu, *J. Phys. Chem. B*, 2005, **109**, 13519.
- 22 F. Xu, Y. N. Lu, Y. Xie and Y. F. Liu, *J. Phys. Chem. C*, 2009, **113**, 1052.
- 23 T. L. Sounart, J. Liu, J. A. Voigt, M. Huo, E. D. Spörcke and B. McKenzie, *J. Am. Chem. Soc.*, 2007, **129**, 15786.
- 24 X. D. Yan, Z. W. Li, C. W. Zou, S. Li, J. Yang, R. Chen, J. Han and W. Gao, *J. Phys. Chem. C*, 2010, **114**, 1436.
- 25 F. Xu, Z. Y. Yuan, G. H. Du, T. Z. Ren, C. Bouvy, M. Halasa and B. L. Su, *Nanotechnology*, 2006, **17**, 588.
- 26 F. Xu, Z. Y. Yuan, G. H. Du, M. Halasa and B. L. Su, *Appl. Phys. A: Mater. Sci. Process.*, 2007, **86**, 181.
- 27 H. B. Lu, H. Li, L. Liao, Y. Tian, M. Shuai, J. C. Li, M. F. Hu, Q. Fu and B. P. Zhu, *Nanotechnology*, 2008, **19**, 045605.
- 28 H. X. Li, Z. F. Bian, J. Zhu, D. Q. Zhang, G. S. Li, Y. N. Huo, H. Li and Y. F. Lu, *J. Am. Chem. Soc.*, 2007, **129**, 8406.
- 29 L. P. Xu, Y. L. Hu, C. Pelligra, C. H. Chen, L. Jin, H. Huang, S. Sithambaram, M. Aindow, R. Joesten and S. L. Suib, *Chem. Mater.*, 2009, **21**, 2875.
- 30 Y. H. Tong, J. Cheng, Y. L. Liu and G. G. Siu, *Scr. Mater.*, 2009, **60**, 1093.
- 31 D. S. Bohle and C. J. Spina, *J. Am. Chem. Soc.*, 2007, **129**, 12380.
- 32 A. Khan, W. M. Jadwisieniczak and M. E. Kordes, *Phys. E.*, 2006, **33**, 331.
- 33 H. B. Zeng, W. P. Cai, Y. Li, J. L. Hu and P. S. Liu, *J. Phys. Chem. B*, 2005, **109**, 18260.
- 34 Y. F. Chen, D. M. Bagnall, H. J. Koh, K. T. Park, K. Hiraga, Z. Q. Zhu and T. Yao, *J. Appl. Phys.*, 1998, **84**, 3912.
- 35 A. B. Djurisic, W. C. H. Choy, V. A. L. Roy, Y. H. Leung, C. Y. Kwong, K. W. Cheah, T. K. G. Rao, W. K. Chan, H. F. Lui and C. Surya, *Adv. Funct. Mater.*, 2004, **14**, 856.
- 36 K. Vanheusden, C. H. Seager, W. L. Warren, D. R. Tallant and J. A. Voigt, *Appl. Phys. Lett.*, 1996, **68**, 403.
- 37 K. Vanheusden, W. L. Warren, C. H. Seager, D. R. Tallant and J. A. Voigt, *J. Appl. Phys.*, 1996, **79**, 7983.
- 38 A. V. Dijken, E. A. Meulenkaamp, D. Vanmaekelbergh and A. Meijerink, *J. Phys. Chem. B*, 2000, **104**, 1715.
- 39 S. B. Zhang, S. H. Wei and A. Zunger, *Phys. Rev. B: Condens. Matter*, 2001, **63**, 075205.
- 40 B. X. Liu, Z. X. Fu and Y. B. Jia, *Appl. Phys. Lett.*, 2001, **79**, 943.
- 41 Y. H. Zheng, C. Q. Chen, Y. Y. Zhan, X. Y. Lin, Q. Zheng, K. M. Wei, J. F. Zhu and Y. J. Zhu, *Inorg. Chem.*, 2007, **46**, 6675.
- 42 H. B. Zeng, G. T. Duan, Y. Li, S. K. Yang, X. X. Xu and W. P. Cai, *Adv. Funct. Mater.*, 2010, **20**, 561.
- 43 A. L. Linsebigler, G. Q. Lu and J. T. Yates, *Chem. Rev.*, 1995, **95**, 735.
- 44 R. W. Matthews, *J. Catal.*, 1986, **97**, 565.
- 45 I. Izumi, W. W. Dunn, K. O. Wilbourn, F. R. F. Fan and A. J. Bard, *J. Phys. Chem.*, 1980, **84**, 3207.
- 46 J. C. Wang, P. Liu, X. Z. Fu, Z. H. Li, W. Han and X. X. Wang, *Langmuir*, 2009, **25**, 1218.
- 47 J. Y. Shi, H. N. Cui, Z. B. Liang, X. H. Lu, Y. X. Tong, C. Y. Su and H. Liu, *Energy Environ. Sci.*, 2011, **4**, 466.